Supporting Information

A novel design of electrolyser using trifunctional (HER/OER/ORR) electrocatalyst for decoupled H_2/O_2 generation and solar to hydrogen conversion

Mingrui Guo, Ling Wang, Jing Zhan, Xiuling Jiao, Dairong Chen and Ting Wang**

School of Chemistry& Chemical Engineering, National Engineering Research Center for Colloidal Materials, Shandong University
E-mail: t54wang@sdu.edu.cn; cdr@sdu.edu.cn

1. Materials

Potassium hydroxide (KOH), sodium hydroxide (NaOH), $CH_3COONa{\cdot}2H_2O$, ethylene glycol, H_3PO_4 (85 wt%), tetra-n-butyl titanate and polyvinyl alcohol were purchased from Sinopharm Chemical Reagent Co. Ltd.. Thiourea was purchased from Tianjin Guangcheng Chemical Factory. Stainless steel mesh (250 mesh) and Ni foams with a thickness of 1.6 mm were purchased from Kunshan Guangjiayuan Electronic Material Co. Ltd.. All the reagents were of analytical grade and used as-received without further purification. Ultrapure water (18.25 MΩ) were used in all experiments. The relay electrodes ($Ni(OH)_2$/NiOOH) were purchased from Jiangsu Haisida Energy Co. Ltd., which are originally used in commercial Ni-MH and Ni-Cd batteries. Silicon solar cells were purchased from Xuneng Trading Company.

2. Characterization

Powder X-ray diffraction (XRD) patterns were collected on a Rigaku D/Max 2200PC diffractometer with a graphite monochromator and Cu Kα radiation (λ= 0.15418 nm). Morphology and microstructure of the products were characterized by a transmission electron microscope (TEM, JEOL JEM-1011) with an accelerating voltage of 100 kV, and a field emission-scanning electron microscope (FE-SEM, SU8010).

3. Synthesis

Synthesis of the NSF/CNT. Ni foams were cleaned through sonication consecutively in concentrated HCl solution (3 M) and acetone for 3 times to remove the NiO_x layer on the surface, then the foams were washed with deionized water and ethanol for 3 times. In a typical synthesis process, the pre-cleaned nickel foams were placed in a ceramic boat located at the center of a tube furnace, and an alumina boat containing 8 g thiourea was placed in the entrance of the furnace as the sources of carbon, sulfur and nitrogen. Before the furnace was heated, Ar (99.99 % in purity) were introduced into the tube furnace system with a flow rate of 100 sccm for 30 min to drive the air out from the tube. Subsequently, the tube was heated up to 900 °C

with a heating speed of 10 °C min^{-1} and kept at that temperature for 1 h. The obtained NSF/CNT were allowed to be cooled to room temperature naturally.

Synthesis of $NaTi_2(PO_4)_3$ electrode. $NaTi_2(PO_4)_3$ were synthesized using a method reported previously.[S1] $CH_3COONa{\cdot}2H_2O$ (4 mmol) was dissolved in 80 mL ethylene glycol and agitated for 0.5 h. 2 mL of H_3PO_4 (85 wt%), and 8 mmol tetra-n-butyl titanate were dropped into the solution, and then stirred for 1 h. The colloidal solution were heated under reflux conditions for 4 h at 180 °C and then cooled to room temperature naturally. The as-obtained white powder (NTP precursor) was collected by centrifugation and washing with deionized water and alcohol for three times and vacuum-dried at 60 °C for 8 h. A one-section tube furnace with a length of 1.5 m was used for the NTP preparation. We placed the NTP precursor powder mixed with polyvinyl alcohol in the center of the alumina ceramic tube (internal and external diameters of 40 cm and 50 cm, respectively). The NTP precursor powder, mixed with polyvinyl alcohol (NTP : PVA = 100 : 15 w/w) were placed in a ceramic boat located at the center of a tube furnace. Before the furnace was heated, Ar (99.99 % in purity) gas were introduced into the tube furnace system. Subsequently, the tube was annealed at 260 °C for 2h, and then heated up to 600 °C for 2 h (heating rate: 3 °C min^{-1}). The obtained carbon-coated NTP were allowed to be cooled down to room temperature naturally. The crystallinity and morphology of the NTP were evaluated by XRD and SEM (Figure SS1). The as-synthesized NTP also shows high capacity with charge capacities of 103 and 85 mAh g^{-1} at 0.5C and 50C (Figure SS2)

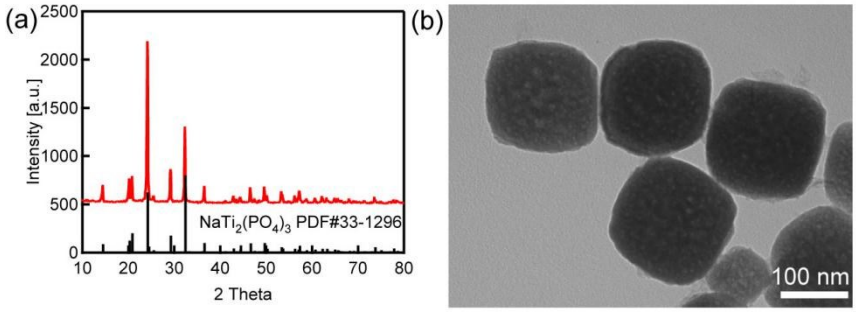

Figure SS1. (a) XRD and (b) SEM images of the NTP.

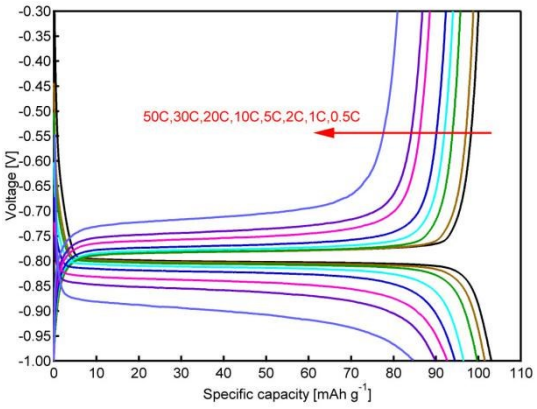

Figure SS2. The charge–discharge curves of NTP at different current rates.

4. Electrochemical measurements

Electrochemical measurements are performed with a CHI 760E electrochemical analyzer (CH Instruments, Inc., Shanghai) in a standard three-electrode system, using the produced products as the working electrode, a graphite rod, an Ag/AgCl working as the counter electrode and the reference electrode, respectively. All HER and OER tests were carried out in N_2-saturated 1 M KOH at room temperature. All the potential values measured were calibrated with respect to reversible hydrogen electrode (RHE) using the Nernst equation: $E_{RHE} = E_{Ag/AgCl} + 0.198 + 0.059pH$. The current density is based on the geometrical area of the working electrode. Linear sweep voltammetry (LSV) data was measured with a scan rate of 2 mV s^{-1}. For oxygen reduction reaction (ORR), the CV profiles were obtained in O_2-saturated 1 M KOH solution at a scan rate of 10 mV s^{-1}. The LSV tests are measured in O_2-saturated 1 M KOH solution at a scan rate of 5 mV s^{-1}.

5. New electrolyser design and fabrication (one-cell configuration)

The designed cell was constructed with the NSF/CNT (1*1cm^2) as the gas evolution electrode (GEE), and the $NaTi_2(PO_4)_3$ (2*2 cm^2) or $Ni(OH)_2$ (3*4 cm^2) as the relay electrode (RE).

One-cell design with $Ni(OH)_2$ as the relay.

The alkaline water electrolysis cell was investigated using chronopotentiometry measurements with applied currents of 100 mA. In the HER process, the GEE electrode (NSF/CNT electrode) and $Ni(OH)_2$ electrode were connected to the cathode and anode of the power source, respectively. The duration time of the H_2-production step is set as 900 s with an applied current of 100 mA, which shows the anodic potential of 0.421 V (versus Ag/AgCl) of the $Ni(OH)_2$ oxidation ($Ni(OH)_2$-NiOOH) and the cathodic potential of -1.098 V (versus Ag/AgCl) of the

H_2O reduction (H_2O-H_2). After HER step, the O_2-production step was initiated by reversing the current polarity, which shows anodic potential (OH^--O_2, 0.476 V vs. Ag/AgCl) and the cathodic potential of NiOOH (0.308 V vs. Ag/AgCl).

One-cell design with $NaTi_2(PO_4)_3$ as the relay.

The alkaline water electrolysis cell was investigated using chronopotentiometry measurements with applied currents of 10 mA. In the OER process, the GEE electrode (NSF/CNT electrode) and $NaTi_2(PO_4)_3$ electrode were connected to the anode and cathode of the power source, respectively. The duration time of the O_2-production step was set as 900 s with an applied current of 10 mA, which shows the anodic potential of approximately 0.418 V (vs. Ag/AgCl) of the oxidation of OH^- (OH^--O_2) and the cathodic potential of -0.812 V (vs. Ag/AgCl) for the sodiation ($Ti^{4+}\rightarrow Ti^{3+}$). After OER step, the H_2-production step was initiated by reversing the current polarity, which shows cathodic potential (H_2O-H_2, -1.109 V vs. Ag/AgCl) and the anodic potential of the desodiation ($Ti^{3+}\rightarrow Ti^{4+}$) (-0.768 V vs. Ag/AgCl).

6. H_2 gas purity and the Faradaic efficiency

An automated in-situ gas evaluation system is used for gas purity measurement (Zhongjiaojinyuan Co. Ltd.). The electrolyser with NSF/CNT (GEE) and $Ni(OH)_2$ (RE) was connected to the gas evaluation system and the H_2/O_2 gas produced in the HER/OER process were delivered into a Gas Chromatography (3420A, BeiFenRuiLi Co., Ltd) using ultrapure Ar gas as the purging gas. For a constant current of 100 mA in a period of～3h (10000 s), the gas obtained from the cell are automatically taken every 15 minutes for detection.

In order to further visualize the production and collection of hydrogen, the electrolyser was also connected to a glass pipe which was prefilled with blue color aqueous solution of methylene blue. As shown in Figure SS3, for cell operation at a constant current of 100 mA, 5 mL of the aqueous solution were evacuated from the pipe within 431 seconds, corresponding to a H_2 generation efficiency of 0.696 mL min^{-1}, and the corresponding Faradic efficiency is ~100 %.

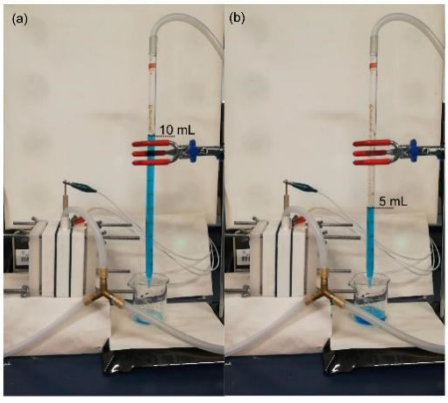

Figure SS3. Photographs showing the amount of the produced H_2 gas.

7. The calculation for the decoupling efficiency and the energy conversion efficiency.

Decoupling efficiency:

$$\eta_{decoup} = \frac{1.48V}{E_{\ cell\ voltage}}$$

As shown in the above equation, the decoupling efficiency can be calculated by dividing the thermoneutral voltage 1.48 V by the practical cell voltage. Figure SS4a, the overall efficiency of the two-step two-electrode decoupled water splitting using the NTP relay was calculated to be 97 % compared to the one-step process, based on a comparison of their operating voltage at a current of 10 mA. The decreased efficiency is mainly owing to the redox potential loss of the RE.

As shown in Figure SS4b, the overall efficiency of the two-step two-electrode decoupled water splitting using the $Ni(OH)_2$ relay was calculated to be 93 % compared to the one-step process, based on a comparison of their operating voltage at a current of 100 mA.

Energy conversion efficiency:

In the process of electrolysis, the heat absorption and heat release are almost equal, and the reaction can be considered in thermoneutral situation. The thermoneutral voltage (E_{tn}) is 1.48V (under conditions T=298 K, 1 atm pressure), calculated by the following equation:

$$E_{tn} = \frac{\Delta H^0}{nF} \quad \text{(Equation S1)}$$

Where the enthalpy change ΔH^0=285.8 kJ mol^{-1}, the number of transferred electrons n=2, the Faradaic constant F=96495 C mol^{-1}. With the Faradaic efficiency near 100 %, the practical energy conversion efficiency can be calculated by dividing the thermoneutral voltage 1.48 V by the practical cell voltage. [S2]

With NSF/CNT as the gas evolution electrode and the NTP as the relay electrode, at current density of 10 mA/cm^2, The practical energy conversion efficiency is 94.3% ($\frac{1.48\text{V}}{1.23\text{V}+0.34\text{V}} \times 100\% = 94.3\%$, dividing the thermoneutral potential by the total cell voltage).

With NSF/CNT as the gas evolution electrode and the $Ni(OH)_2$ as the relay electrode, at current of 100 mA, The practical energy conversion efficiency is 87.6 % ($\frac{1.48\text{V}}{0.17\text{V}+1.52\text{V}} \times 100\% = 87.6\%$).

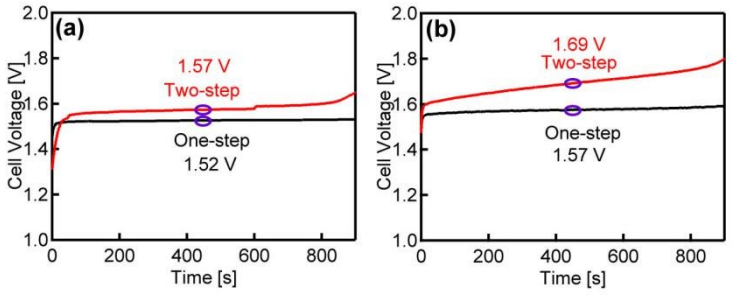

Figure SS4. Cell voltages versus time for one-step system and the add-up of two-step system. (a) Driven voltage comparison at 10mA using NTP relay electrode. (b) Driven voltage comparison at 100mA using $Ni(OH)_2$ relay electrode.

8. PV-powered decoupled water splitting using a commercial Si PV module and the design of a two-cell electrolyser

A two-cell electrolyser was constructed with cell 1 and cell 2 contains the same GEE electrodes (Figure S1), and the relay electrodes ($Ni(OH)_2$) in two cells are connected by a copper wire. The cells are fully filled with 1M KOH aqueous electrolyte solution and the electrodes are all immersed in the electrolytes.

The PV-electrolysis system is shown in Figure S10. The area of the Si PV cell was 4 × 3.6 cm^2. The efficiency of the solar cell (η_{PV}) is defined as the quotient of maximum power output of the solar cell (P_{max}) and the power input from the light source (P_{in}).[S3]

$$\eta_{PV} = \frac{P_{max}}{A \cdot P_{in}} = \frac{I_{SC} \cdot V_{OC} \cdot FF}{A \cdot P_{in}} = \frac{I_{SC} \cdot V_{OC} \cdot \frac{I_{MP} \cdot V_{MP}}{I_{SC} \cdot V_{OC}}}{A \cdot P_{in}} = \frac{I_{MP} \cdot V_{MP}}{A \cdot P_{in}} \quad \text{(Equation S2)}$$

P_{max} is the product of short circuit current (I_{SC}), open circuit voltage (V_{OC}) and fill factor (FF) of the solar cell, which is defined as the quotient of the products of current (I_{MP}) and voltage (V_{MP}) at the maximum power point and I_{SC} and V_{OC}. The calculated efficiency of the commercial Si PV module is 14.4 %.

One terminal of the Si PV module was connected to the GEE (NSF/CNT) electrode in cell 1, and the other terminal of the Si PV module was connected to the GEE (NSF/CNT) electrode in cell 2. The RE ($Ni(OH)_2$/NiOOH) electrodes in two cells were connected to each other through a copper wire. Solar water splitting was carried out by illuminating the PV module with simulated solar radiation (calibrated to 100 mW/cm^2) from a Xenon light source (CEL-HXF300, Beijing zhongjiao jinyuan technology Co. Ltd.), or illuminated under real sunlight.

Supplementary Figures:

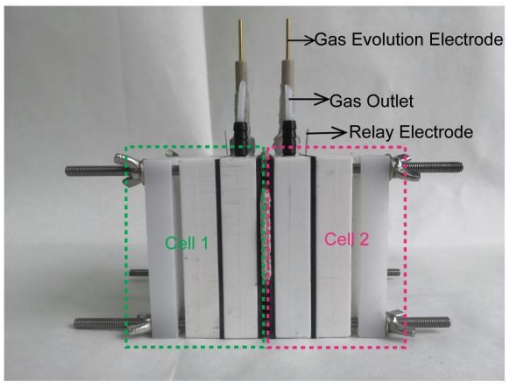

Figure S1. The photograph of an electrolyser for decoupled water splitting with one-cell or two-cell configuration.

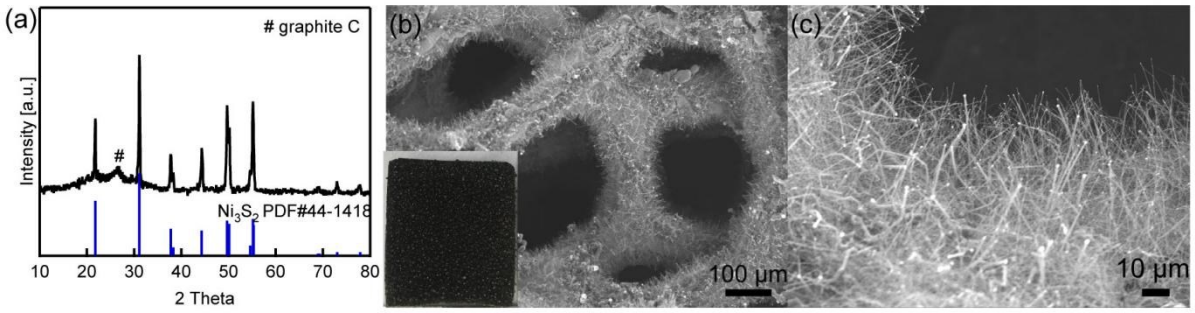

Figure S2. (a)XRD and (b, c) SEM images of the NSF/CNT (the inset in SEM is a photograph of the NSF/CNT).

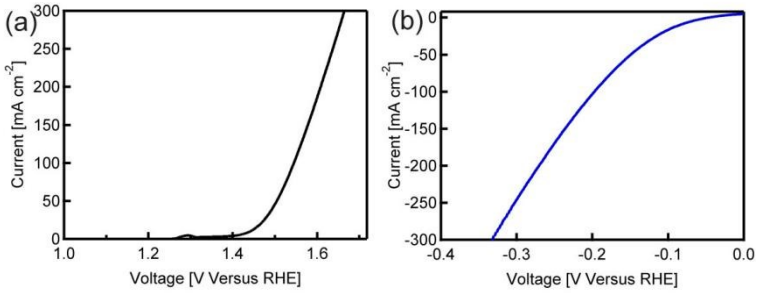

Figure S3. Linear sweep voltammetry curve of the (a) OER and (b) HER for the NSF/CNT in N_2 saturated 1 M KOH.

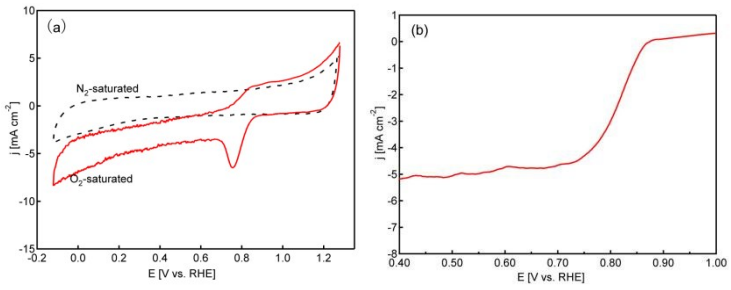

Figure S4. (a) Cyclic voltammetry curves of NSF/CNT in N_2- and O_2-saturated electrolytes (1 M KOH), (b) Linear sweep voltammetry curve.

Figure S5. The photo profile of the $Ni(OH)_2$ electrode (3 * 4 cm^2)

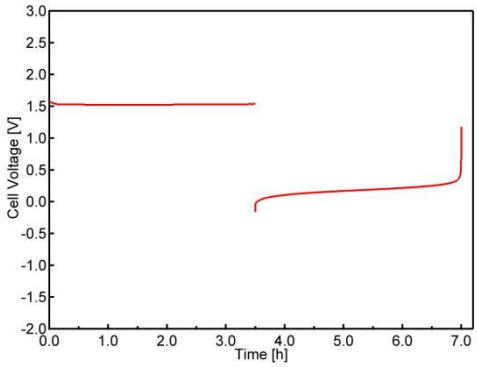

Figure S6. At a constant current of 100 mA, cell potential versus time showing a sudden potential increase after operation for 3.5 h, which indicates the NiOOH are completely converted into $Ni(OH)_2$ at this point.

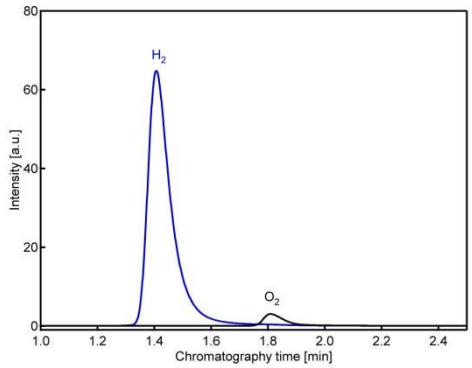

Figure S7. The GC signals for pure H_2 and O_2 gas in the in-situ GC system with Ar as the carrier gas.

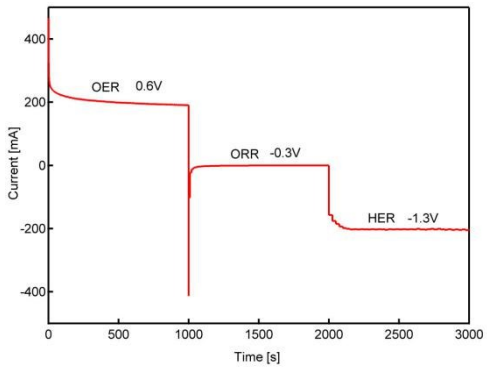

Figure S8. The current-time curve of multi-potential steps at different voltages (vs. Ag/AgCl) for the operation of OER-ORR-HER steps.

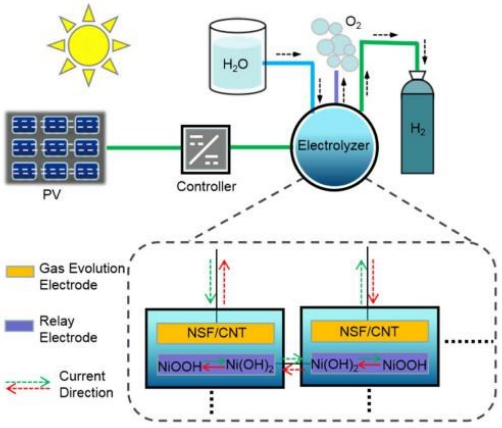

Figure S9. Schematic illustration showing the solar water splitting system.

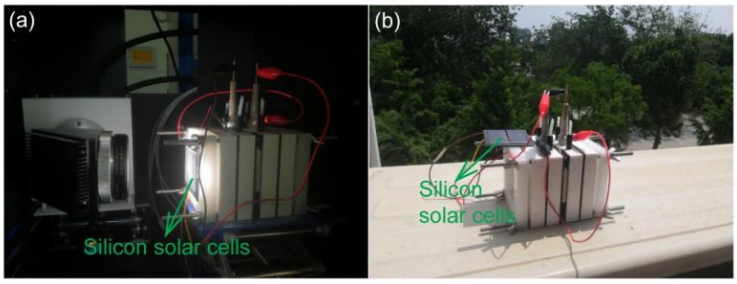

Figure S10. The photograph of the PV-electrolysis system. (a) Solar water splitting using simulated solar radiation (100 mW/cm^2). (b) Solar water splitting under real solar light.

Table S1. Comparison of our new design of the electrolyser for decoupled water splitting with reported decoupled water splitting systems with different relay mediators.

Relay mediators	Redox peaks	Electrolyte	Electrocatalyst	Membrane/ diaphragm	Two-step cell Voltage @ j/area	One-step cell Voltage @ j/area	Decoupling efficiency (%)	Energy efficiency (%)	Ref
$Na_3Ti_2(PO_4)_3$/ $NaTi_2(PO_4)_3$	-0.838/-0.756 $V_{Ag/AgCl}$	1 M NaOH	NSF/CNT for HER and OER	NO	1.57V@ 10mA/cm^2	1.52V@ 10mA/cm^2	97	94.3	This work
$Ni(OH)_2$/ NiOOH	0.423/0.238 $V_{Ag/AgCl}$	1 M NaOH	NSF/CNT for HER and OER	NO	1.69V@ 100mA/6cm^2	1.57V@ 100mA/6cm^2	93	87.6	
$H_3PMo_{12}O_{40}$	0.65 V_{NHE}	1 M H_3PO_4	Pt for HER, Pt for OER, carbon felt for ECPB	PEM[1]	2.94V@ 100 mA/cm^2	2.55V@ 100mA/cm^2	86.7	50.3	S4
$H_4[SiW_{12}O_{40}]$	0.01/-0.22 V_{NHE}	1 M H_3PO_4	Pt/C for HER, Pt for OER, carbon felt for ECPB	PEM	2.37V@ 50mA/cm^2	2.21V@ 50mA/cm^2	93.2	63	S5
Hydroquinone sulfonate	0.7/0.65 V_{NHE}	1.8 M H_3PO_4	Pt for HER, Pt for OER, carbon felt for ECPB	PEM	3.29V@ 50mA/cm^2	2.62V@ 50mA/cm^2	80	45	S6
V-Ce RFB	V(III)/V(II) 0.25 V_{SHE} Ce(IV)/Ce(III) 1.52 V_{SHE}	1 M H_2SO_4	Mo_2C for HER, IrO_2/RuO_2 for OER	PEM				48	S7
$H_3PMo_{12}O_{40}$	0.65 to 1.18 V_{NHE}	1 M CH_3SO_3H	WO_3 photoanodes for OER, Pt mesh for HER, carbon felt for ECPB	PEM					S8
$Ni(OH)_2$/NiOOH	0.43/0.49 $V_{Hg/HgO}$	1 M KOH	Pt for HER, RuO_2/IrO_2 for OER	NO	2V@ 200mA/10cm^2	1.829V@ 200mA/10cm^2	91.5	74	S9
			Co_3O_4 for OER, Ni-foam for HER		2.137V@ 200mA/10cm^2	1.973V@ 200mA/10cm^2	92.3	69.3	
$Ni(OH)_2$/NiOOH	1.36 V_{RHE}	1 M NaOH	Pt for HER, Ir for OER	NO	2.21V@ 128 mA	2.047V@ 128 mA	92.6	58	S10
			Ni foil for HER, Ni foil for OER		2.12V@ 2mA/cm^2	2V@ 2mA/cm^2	94.3	56	
$Na_4[Fe(CN)_6]$	0.9 V_{RHE}	0.5 M Na_2SO_4 and 0.5 M	Co-P for HER, Ni for OER, carbon electrode for $Na_4[Fe(CN)_6]$	Cation exchange membrane	2.29V@ 10mA/cm^2	2.27V@ 10mA/cm^2	99	64.6	S2

		NaPi buffer							
FcNCl	0.4 $V_{Ag/AgCl}$	0.5 M Na_2SO_4	Ni_2P/Ni for HER Ni for OER, carbon electrode for redox of FcNCl		2.43V@ 10mA/cm^2	2.338V@ 10mA/cm^2	96.2	60.9	
Polytriphenylamine	0.5/0.48 $V_{Ag/AgCl}$ 0.6 /0.58 $V_{Ag/AgCl}$	0.5M H_2SO_4	Pt for HER RuO_2/IrO_2 for OER	NO	1.65V@ 5mA/3cm^2	1.6V@ 5mA/3cm^2	97	89.7	S11
					2.22V@ 100mA/3cm^2			66.7	
pyrene-4,5,9,10-tetraone	0.34/0.2 $V_{Ag/AgCl}$ 0.46 /0.32 $V_{Ag/AgCl}$	0.5M H_2SO_4	Pt for HER RuO_2/IrO_2 for OER	NO	1.66V@ 5mA/cm^2	1.57V@ 5mA/cm^2	94.6	89.2	S12
					1.87V@ 50mA/cm^2	1.76V@ 50mA/cm^2	94	79	
polyaniline	0.39 to 0.85 V_{RHE}	0.5 M H_2SO_4	Pt for HER RuO_2/IrO_2 for OER	NO	1.92V@ 50mA/cm^2	1.73V@ 50mA/cm^2	90	77	S13
$Na_{0.44}MnO_2$	−0.2 to 0.55 $V_{Hg/HgO}$	1 M NaOH and saturated NaCl	Pt for HER RuO_2/IrO_2 for CER	NO	2.37V@ 100mA/10cm^2	2.24V@ 100mA/10cm^2	94.5	62.4	S14
$Ni_{0.9}Co_{0.1}(OH)_2$	1.31 to 1.41 V_{RHE}	5 M KOH	Platinized nickel for HER, T=95 °C spontaneous oxygen release	NO	1.44V@ 10mA/cm^2				S15
					1.56V@ 100mA/cm^2				

1. PEM: proton exchange membrane.

References

S1. Hu, Q.; Liao, J. Y.; Li, C. T.; He, X. D.; Ding, X.; Chen, C. H., Synthesis of porous carbon-coated $NaTi_2(PO_4)_3$ nanocubes with a high-yield and superior rate properties. *Journal of Materials Chemistry A* **2018**, *6* (47), 24503-24508.

S2. Li, W.; Jiang, N.; Hu, B.; Liu, X.; Song, F.; Han, G.; Sun, Y., Electrolyzer design for flexible decoupled water splitting and organic upgrading with electron reservoirs. *Chem* **2018**, *4* (3), 637-649.

S3. Bonke, S. A.; Wiechen, M.; MacFarlane, D. R.; Spiccia, L., Renewable fuels from concentrated solar power: towards practical artificial photosynthesis. *Energy & Environmental Science* **2015**, *8* (9), 2791-2796.

S4. Symes, M. D.; Cronin, L., Decoupling hydrogen and oxygen evolution during electrolytic water splitting using an electron-coupled-proton buffer. *Nature chemistry* **2013**, *5* (5), 403.

S5. Rausch, B.; Symes, M. D.; Chisholm, G.; Cronin, L., Decoupled catalytic hydrogen evolution from a molecular metal oxide redox mediator in water splitting. *Science* **2014**, *345* (6202), 1326-1330.

S6. Rausch, B.; Symes, M. D.; Cronin, L., A bio-inspired, small molecule electron-coupled-proton buffer for decoupling the half-reactions of electrolytic water splitting. *Journal of the American Chemical Society* **2013**, *135* (37), 13656-13659.

S7. Amstutz, V.; Toghill, K. E.; Powlesland, F.; Vrubel, H.; Comninellis, C.; Hu, X.; Girault, H. H., Renewable hydrogen generation from a dual-circuit redox flow battery. *Energy & Environmental Science* **2014**, *7* (7), 2350-2358.

S8. Bloor, L. G.; Solarska, R.; Bienkowski, K.; Kulesza, P. J.; Augustynski, J.; Symes, M. D.; Cronin, L., Solar-driven water oxidation and decoupled hydrogen production mediated by an electron-coupled-proton buffer. *Journal of the American Chemical Society* **2016**, *138* (21), 6707-6710.

S9. Chen, L.; Dong, X.; Wang, Y.; Xia, Y., Separating hydrogen and oxygen evolution in alkaline water electrolysis using nickel hydroxide. *Nature communications* **2016**, *7* (1), 1-8.

S10. Landman, A.; Dotan, H.; Shter, G. E.; Wullenkord, M.; Houaijia, A.; Maljusch, A.; Rothschild, A., Photoelectrochemical water splitting in separate oxygen and hydrogen cells. *Nature materials* **2017**, *16* (6), 646-651.

S11. Ma, Y.; Dong, X.; Wang, Y.; Xia, Y., Decoupling Hydrogen and Oxygen Production in Acidic Water Electrolysis Using a Polytriphenylamine-Based Battery Electrode. *Angewandte Chemie International Edition* **2018**, *57* (11), 2904-2908.

S12. Ma, Y.; Guo, Z.; Dong, X.; Wang, Y.; Xia, Y., Organic Proton-Buffer Electrode to Separate Hydrogen and Oxygen Evolution in Acid Water Electrolysis. *Angewandte Chemie International Edition* **2019**, *58* (14), 4622-4626.

S13. Wang, J.; Ji, L.; Teng, X.; Liu, Y.; Guo, L.; Chen, Z., Decoupling half-reactions of electrolytic water splitting by integrating a polyaniline electrode. *Journal of Materials Chemistry A* **2019**, *7* (21), 13149-13153.

S14. Hou, M.; Chen, L.; Guo, Z.; Dong, X.; Wang, Y.; Xia, Y., A clean and membrane-free chlor-alkali process with decoupled Cl_2 and H_2/NaOH production. *Nature communications* **2018**, *9* (1), 1-8.

S15. Dotan, H.; Landman, A.; Sheehan, S. W.; Malviya, K. D.; Shter, G. E.; Grave, D. A.; Hadari, N., Decoupled hydrogen and oxygen evolution by a two-step electrochemical–chemical cycle for efficient overall water splitting. *Nature Energy* **2019**, *4* (9), 786-795.